Investigation of mechanical properties, photons, neutrons, and charged particles shielding characteristics of Bi_2O_3/B_2O_3/SiO_2 glasses

I. O. Olarinoye[1] · F. I. El-Agawany[2] · A. Gamal[2] · El Sayed Yousef[3,4] · Y. S. Rammah[2]

Abstract

Mechanical properties, uncharged and charged particles shielding capacity of $60Bi_2O_3$-(40-x) B_2O_3-$xSiO_2$: $x = 0$ (S1), 10 (S2), 20 (S3), 30 (S4), and 40 (S5) mol% glasses have been investigated. The enhancement in Young's, shear, and longitudinal elastic moduli and Poisson's ratio of the denser Bi content of the S-glasses was confirmed via bond compression (B–C) and Makishima–Mackenzie (M–M) models. The trend order of the mass attenuation coefficient (MAC) is consistent with that of the mass density as $(S1)_{MAC} < (S2)_{MAC} < (S3)_{MAC} < (S4)_{MAC} < (S5)_{MAC}$. The highest value of the linear attenuation coefficients (LAC) for each of the S-glasses was obtained at photon energy of 15 keV with values of 601, 624, 640, 648, and 661 cm^{-1} for S1–S5, respectively. The increasing trend of the mean free path (MFP) is opposite to that of MAC and LAC with the order: $(S1)_{MFP} > (S2)_{MFP} > (S3)_{MFP} > (S4)_{MFP} > (S5)_{MFP}$. The maximum tenth value thickness (TVT) of the glasses was recorded at 4 MeV with values of 3.93, 3.79, 3.70, 3.67, and 3.60 cm for S1, S2, S3, S4, and S5, respectively. The trend of the effective atomic number (Z_{eff}) directly follows the MAC. Both exposure and energy absorption buildup factors (EBUF and EABUF) were increased with photon energy and depth of penetration except at Bi absorption edges where spikes were seen. Comparing the effective linear attenuation coefficient (ELAC) of the glasses, it is affirmed that S5 has the greatest photon absorption coefficient for all the considered energy and depth. Therefore, the S-glasses are better photon absorber and will perform better in gamma radiation shielding in nuclear facilities compared to commercially available glass shields (RS360 and RS520) and a recently investigated glass matrix (TVM60). In addition, the glass system can thus be used for fast neutron absorber rather than ordinary concrete or water.

Keywords Borate glasses · Mechanical properties · Radiation shielding · MAC · ELAC

1 Introduction

Due to ease of production, low cost, and ability to be shaped into different shapes, glass has over the years become one of the commonest materials with diverse applications in different human societies. Today, glass is used to manufacture everyday household items, optical devices, for aesthetics, and as building material. Glasses are also used for optical coatings, semiconductors, microelectronics, radiation detectors, nuclear waste management, telecommunication, photonics, and many more advanced applications [1–5]. The use of glass for a particular purpose is a function of its chemical composition which in turn dictates its physical, mechanical, and other useful properties. The ease of fine-tuning the chemical composition of glasses have produced novel glasses with more useful applications that have continued to grow. One of the fast-growing areas of application is for

✉ Y. S. Rammah
dr_yasser1974@yahoo.com

1 Department of Physics, School of Physical Sciences, Federal University of Technology, Minna, Nigeria

2 Physics Department, Faculty of Science, Menoufia University, Shebin El Koom 32511, Egypt

3 Research Center for Advanced Materials Science (RCAMS), King Khalid University, P. O. Box 9004, Abha 61413, Saudi Arabia

4 Physics Dep, Faculty of Science, King Khalid University, P. O. Box 9004, Abha 61413, Saudi Arabia

ionizing radiation shielding [6–10]. The synthesis and radiation shielding characterization of glass materials has continued to gain worldwide attention among research and material science communities [11–15]. This is because of the strong radiation shielding potential shown by many investigated glass compositions [16–25]. To this end, many glass species have been recommended for shielding application while some have been fabricated and commercialized for ionizing radiation shielding purposes under different brand names. One major take away from the many research into radiation shielding studies of glasses is that the shielding capacity of a glass against a particular radiation type and energy depends strongly on its chemical composition [6, 11, 26–30]. Using the glass for source or structural shield in a particular facility would further rely on its physical and mechanical characterization. Consequently, studies on the shielding potential of glasses are incomplete without discussions on their mechanical and physical features.

Ionizing radiation is broadly classified into uncharged and charged radiations like photons, neutrons, electrons, and heavy charged particles. Out of these, of major concern to radiation shielding engineers are neutrons and photons [31–40]. This is due to their high penetration ability. Thus, the classification of a glass as good shielding materials must include assessment of its neutron and photon shielding parameters [35, 38–42]. While effective photon shields are expected to be dense and have high mass attenuation coefficient, on the other hand, neutron shield simply require that the shield hold high neutron absorbing elements such as H, B, Li, and Cd. Thus, for glasses that are needed as shields in a mixed radiation field comprising of both photons and neutrons, its composition must strike a balance between light and heavy elements. Hence, the composition of the glass shield would determine the type of radiation, it has a potential of adequately shielding.

The presence of heavy metal oxides (HMO) such has PbO, Bi_2O_3, MoO3, WO_3, and BaO in different glass matrices has produced improvement in the photon shielding effectiveness of the glasses [6–19, 23, 29, 32, 40, 43].

In this study, we investigate the mechanical properties, electron, proton, photon, alpha particle, proton, fast, and thermal neutron shielding capacity of $60Bi_2O_3$-(40-x) B_2O_3-$xSiO_2$ glasses.

2 Materials and methods

2.1 Materials

Five samples of bismuth boron-silicate glasses of the form $60Bi_2O_3$–(40-x) B_2O_3–$xSiO_2$: x = 0, 10, 20, 30, and 40 mol%) were chosen from Ref. [44]. The chosen samples

were named in general as S-glasses and individually as follows:

S1 for $60Bi_2O_3$–$40B_2O_3$-$0SiO_2$ mol%,

S2 for $60Bi_2O_3$–$30B_2O_3$-$10SiO_2$ mol%,

S3 for $60Bi_2O_3$–$20B_2O_3$-$20SiO_2$ mol%,

S4 for $60Bi_2O_3$–$10B_2O_3$-$30SiO_2$ mol%, and,

S5 for $60Bi_2O_3$–$0B_2O_3$-$40SiO_2$ mol%

Sample's code, compositions, density, and molar volume of S1–S5 glasses are tabulated in Table 1.

2.2 Calculation of mechanical properties

In the present work, the mechanical properties include bulk, Young's, shear, and longitudinal elastic moduli and Poisson's ratio of the investigated S1–S5 glasses were evaluated via bond compression (B–C) and Makishima–Mackenzie (M–M) models as in previous articles [28, 43, 45]. The used parameters for calculation process are tabulated in Tables.

2.3 Interaction of photons, neutrons, and charged particles with matter

2.3.1 Photons

The transmission of a narrow beam of photons (x- and gamma-rays) through an absorbing material of thickness d is described via Eq. (1).

$$X = X_o e^{-\mu d} \tag{1}$$

where X_o, X, and μ are the photon energy/particle flux or any measurable photon transmission quantity before and after passing from the irradiated material and the linear attenuation coefficient (LAC) of the said medium, respectively. LAC is a measure of the photon flux that penetrates absorbing medium without interaction. It thus expresses the photon absorption ability of the absorber. Many more parameters can be used to measure the photon absorbing ability of a shield. Mass attenuation coefficient (MAC), mean free path (MFP), half-value thickness (HVT), tenth value thickness

Table 1 Code, chemical composition, and density of the $60Bi_2O_3$-(40-x) B_2O_3-$xSiO_2$: x = 0, 10, 20, 30, and 40 mol%) glasses

Sample code	Composition, (mol%) [44]			Density, ρ (g/cm^3) ± 0.001 [44]	Molar volume, V_m (cm^3/mol) [44]
	SiO_2	B_2O_3	Bi_2O_3		
S1	0	40	60	6.3298	48.5668
S2	10	30	60	6.5527	46.7691
S3	20	20	60	6.6948	45.6339
S4	30	10	60	6.7449	45.1535
S5	40	0	60	6.8550	44.2891

(TVT), and the effective atomic number (Z_{eff}) are some of these parameters. They are related to LAC according to Eqs. (2, 3, 4, 5. 6) [28, 46]:

$$MAC = \frac{LAC}{\rho} \tag{2}$$

$$MFP = {}^{1}/_{LAC} \tag{3}$$

$$HVT = {}^{\ln 2}/_{LAC} \tag{4}$$

$$TVT = {}^{\ln 10}/_{LAC} \tag{5}$$

$$Z_{eff} = \frac{\sum_i w_i A_i (MAC)_i}{\sum_i w_i \frac{A_i}{Z_i}(MAC)_i} \tag{6}$$

where w_i, Z_i, and A_i is the weight fraction, atomic and mass number of the ith elemental component of the absorbing material.

In this current investigation, the MAC values of S1–S5 glass samples were estimated via the WinXCOM [47] computer code for photon energies between 0.015 and 15 meV. Based on Eqs. (2, 3, 4, 5. 6), LAC, HVT, TVT, MFP, and Z_{eff} of the glasses were calculated.

In practical situations, where there is always a deviation from narrow beam transmission of photons, the transmitted photon flux comprises primary and secondary (scattered) photons. Hence, Eq. (1) is adjusted to take care of the contribution due to the scattered photons. To do this, a nondimensional multiplying factor (called photon buildup factor of the radiation quantity X) B_X is added to Eq. (1) as follows:

$$X = X_o B_X e^{-\mu t} \tag{7}$$

where B_X is the photon buildup factor of the radiation quantity X. $B_X = 1$ for idealized narrow beam (good transmission) geometry. B_X was explained in more details and much published articles mentioned and discussed the methods of estimating it and can be found in [48–50]. The calculated values of B_X can be used to correct the value of LAC according to Eq. (8).

$$ELAC(E,x) = LAC(E,d) - \frac{\ln B_X(E,x)}{d} \tag{8}$$

where $x = d*LAC$

ELAC is called the effective linear attenuation coefficient [51]. Just like LAC, ELAC depends on photon energy and materials thickness x (in MFP). The buildup factors for exposure (EBUF) and energy absorption (EABUF) in the S1–S5 glasses were calculated for selected depth up to 40 MFP via the EXABCal computer code [49].

2.3.2 Neutrons

The relative neutron shielding efficacy of a medium may be described using proper microscopic and macroscopic cross sections depending on the class/energy of neutrons of interest. For fast neutrons, the fast neutron removal cross section (FNRC $- \Sigma_R$) which is the macroscopic cross section for fast neutrons may be used. While for thermal neutrons, the microscopic scattering and absorption cross section may be adopted. *FNRC* is almost constant for neutrons having energies in the range of 2 to 12 meV. It can be calculated for glass via the equation [52, 53]:

$$\Sigma_R = \rho \sum w_i \left(\frac{\Sigma_R}{\rho}\right)_i \tag{9}$$

where ρ, w_i, and $\left(\frac{\Sigma_R}{\rho}\right)_i$ is the mass density of the glass, weight fraction, and mass removal cross section of the ith element in it. $\frac{\Sigma_R}{\rho}$ is a smooth function of atomic number, thus for constituent elements of any glass medium, it may be calculated through their atomic numbers, Z as follows:

$$\frac{\Sigma_R}{\rho} = 0.19 Z^{-0.743} \ for \ Z \le 8; \tag{10}$$

and,

$$\frac{\Sigma_R}{\rho} = 0.125 Z^{-0.565} \ for \ Z > 8 \tag{11}$$

Σ_R of S1–S5 glasses were estimated via Eqs. 9, 10, and 11.

Total macroscopic cross section Σ_T (cm^{-1}) of the glasses were calculated through Eq. 12 as found in [54–56]:

$$\Sigma_T = 6.02 \times 10^{23} \rho \sum_i \frac{w_i}{M_i}(\sigma_T)_i \tag{12}$$

where σ_T (cm^2) is the total microscopic cross section.

2.3.3 Electron and proton

The stopping powers and range of charged particles are some of the parameters that can be used to assess their interactions with any medium. Total stopping powers (TSP) and range (R) of electron and proton in S1–S5 glasses were evaluated using ESTAR and SRIM-2013 software [57, 58], respectively.

Table 2 Values of total number of cationic per glass formula unit (η), average cross-link density ($\overline{n}_c$), average stretching force constant ($\overline{F}$), number of network bond per unit volume (n_b), average bond length (l), calculated bond compression elastic moduli (bulk (K_{B-C}), shear (S_{B-C}), longitudinal (L_{B-C}), Young's (E_{B-C})) and Poisson's ratio (σ_{B-C}) of S1–S5 glasses

| Parameters and elastic moduli	S1	S2	S3	S4	S5
η	2	1.9	1.8	1.7	1.6
$\overline{n}_c = \frac{1}{\eta} \sum x_i(n_c)_i(N_C)_i$	0.5	0.578	0.666	0.764	0.875
$\overline{F} = \frac{\sum (xn_f f)_i}{\sum (xn_f)_i} (N/m)$	393.60	372.77	353.25	334.90	317.64
$n_b = \frac{N_A}{V_m} \sum (n_f x)_i \times 10^{28}$ (m^{-3})	3.74	3.99	4.22	4.40	4.62
$l = \left(0.0106 \frac{\overline{F}}{K_{B-C}}\right)^{0.26}$ (nm)	0.48	0.47	0.46	0.45	0.44
$K_{B-C} = \frac{N_A}{9V_m} \sum_i (n_f x \overline{F} r^2)$ (GPa)	68.61	70.87	72.19	72.47	73.32
$S_{B-C} = \left(\frac{3}{2}\right) K_{B-C} \left(\frac{1-2\sigma_{B-C}}{1+\sigma_{B-C}}\right)$ (GPa)	25.79	28.81	31.43	33.55	35.90
$L_{B-C} = K_{B-C} + \frac{4}{3} S_{B-C}$ (GPa)	102.91	109.19	114.01	117.10	121.08
$E_{B-C} = 2S_{B-C}(1 + \sigma_{B-C})$ (GPa)	68.76	76.12	82.36	87.21	92.61
$\sigma_{B-C} = 0.28(\overline{n}_c)^{-0.25}$	0.33	0.32	0.30	0.29	0.28
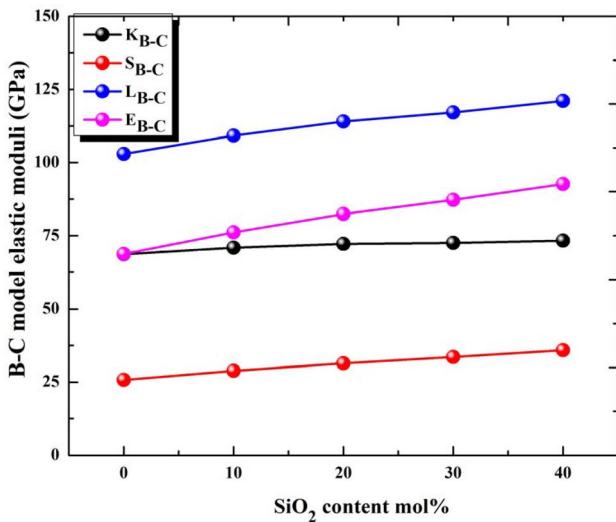
Fig. 1 Elastic moduli via bond compression (B–C) model of S1–S5 glasses

3 Results and discussion

3.1 Elastic moduli of S1–S5 glasses

As shown in Table 2 and Fig. 1, the increase in modulus of elasticity may be due to the substitution of B$_2$O$_3$ (coordination number = 3) by SiO$_2$ which have the coordination number of 4 which leads to the increase of total number of bonds. Theoretically, values of bond compression bulk elastic modulus (K_{B-C}) were found to increase from 68.61 to 73.32 GPa. This increase in (K_{B-C}) can be interpret based on the dependence of the (K_{B-C}) on the number of the network bonds per unit volume (n_b) and the average bond lengths (l), which is related to the first order stretching force constant

Table 3 Coordination number per cation (n_f), cross-link density per cation (n_c), Stretching force constant (F), packing density factor (V_i), and dissociation/bond energy per unit volume (G_i) of the oxides SiO$_2$–B$_2$O$_3$–Bi$_2$O$_3$

Oxide	n_f	n_c	F (N/m)	V_i (m^3/mol)	$G_i \times 10^6$ (KJ/m^3)
SiO$_2$	4	2	432	13.6	68
B$_2$O$_3$	3	1	660	15.2	22.6
Bi$_2$O$_3$	3	1	216	26.1	31.6

($\overline{F}$) [45]. The addition of SiO$_2$ causes (n_b) to increase from 3.7 to 4.6 ($\times 10^{28}$(m^{-3})) despite of the increases in the average stretching force constant from 393.6 to 3.17.6 (N/m). Also, the average cross-link density ($\overline{n}_c$) increases from 0.5 to 0.87 due to the higher coordination number of SiO$_2$. Values of bond compression elastic moduli (shear (S_{B-C}), longitudinal (L_{B-C}), and Young's (E_{B-C})) were found to increase from 25.79 to 35.90 GPa, from 102.91 to 121.08 GPa and from 68.76 to 92.61 GPa, respectively. Values of theoretical Poisson's ratio (σ_{B-C}) were also found to decrease from 0.33 to 0.28 which is due to the increase of average cross-linking density.

The second theoretical treatment for calculating the moduli of elasticity of oxide glasses is based on the Makishima and Mackenzie (M-M) model [28, 43, 45]. As in Table 3, coordination number per cation (n_f), cross-link density per cation (n_c), stretching force constant (F), packing density factor (V_i), and dissociation/bond energy per unit volume (G_i) of the oxides SiO$_2$, B$_2$O$_3$, and Bi$_2$O$_3$ are recorded. Figure 2 and Table 4 show the values of the total packing density (V_t), total dissociation energy (G_t), (Young's (E_{M-M}), bulk (K_{M-M}), and shear (S_{M-M})) elastic moduli, and Poisson's ratio (σ_{M-M}). It was clear that, the increasing in the total packing density of the glass from 0.44 to 0.47 which is attributed to
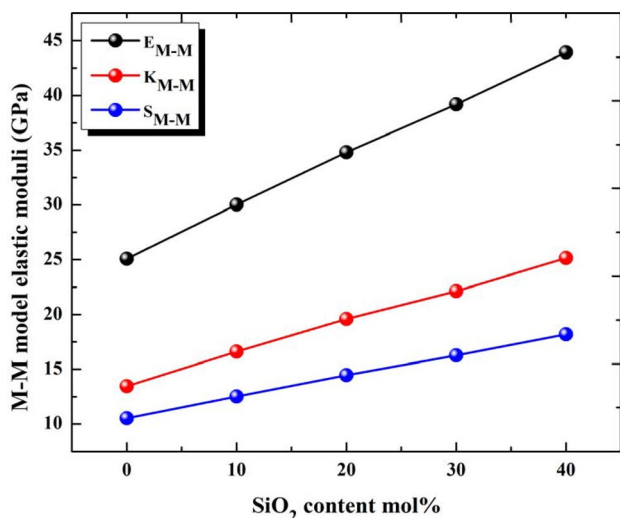
Fig. 2 Elastic moduli via Makishima–Mackenzie (M-M) model of S1–S5 glasses

the higher value of ionic radius of SiO_2 than B_2O_3. Increasing the SiO_2 increases the total dissociation energy per unit volume of the system from 28 to 46.16 kJ/cm^3. This is due to the substitution of B_2O_3 which have dissociation energy (22.6) by SiO_2 which have dissociation energy (68 kJ/cm^3). The calculated values of (E_{M-M}), (K_{M-M}), and (S_{M-M}) were increased from 25.6 to 43.98 (GPa), from 13.46 to 25.14 (GPa), and from 10.53 to 18.19 (GPa), respectively. This behavior is like the increasing behavior of the corresponding moduli measured by bond compression model which are in good agreement.

4 Radiation shielding parameters of S1–S5 glasses

4.1 Photons

Results of mass attenuation coefficients (MAC) of the investigated S-glasses and its variation with photon energy in 0.015–15 MeV range are shown in Fig. 3. From the figure, MAC values vary with energy in common patterns in the glasses. Recorded MAC values for each glass were maximum at 15 keV with corresponding values of 949, 953, 956, 960, and 964 cm^2/g for S1, S2, S3, S4, S5, respectively. Beyond 15 keV, the mass attenuation coefficient of each glass dropped sharply with energy up to an energy of 800 keV after which the decrease slowed down. The slow decrement in MAC values continues up to 4 MeV. Beyond 4 MeV, MAC values start a gradual increase as photon energy increase further. This behavior of MAC is attributed to the photon interaction modes whose interaction cross sections have maximum values at different photon energies. The initial rapid drop in MAC value was due to the dominance of the photoelectric effect. The photoelectric absorption cross section is dominant in the low energies below 800 keV, however, it changes inversely as the fourth power of the photon energy. In the energy range between 0.8 and 4 MeV, the incoherent scattering process dominates the interaction mode. The incoherent scattering cross section changes inversely with energy and thus the MAC values decrease slowly as energy increases. The subsequent gradual increase in MAC values is due to the pair production absorption process. This process is dominant in the energies beyond 4 MeV and the fact that its cross section increases slowly with increase in energy explains why MAC values of the glasses increased steadily with photon energy. The nuclear pair production cross section has an energy threshold of 1.022 MeV but becomes significant at energies beyond 4 MeV. Furthermore, a sharp peak at 0.1 MeV is seen on the MAC spectra. This distinguishable peak is attributed to the K-x-ray absorption of Bi atom. The constant molar concentration of Bi_2O_3 in all the studied glass samples ensures that this peak was found and seen in all the MAC spectra. The intensity of the peak increases as the mass concentration of Bi increases in the glass samples (Table 1). Throughout the energy spectrum considered, the MAC values vary slightly according to the order S1 < S2 < S3 < S4 < S5. However, this difference is more prominent in the low energy region where the photoelectric effect is most dominant. The trend

Table 4 Total ionic packing density (V_t), total dissociation energy (G_t), Young's modulus (E_{M-M}), bulk modulus (K_{M-M}), shear modulus (S_{M-M}), and Poisson's ratio (σ_{M-M}) based on Makishima–Mackenzie model of S1–S5 glasses

Parameters and elastic moduli	S1	S2	S3	S4	S5
$V_t = \left(\frac{1}{V_m}\right) \sum_i (V_i x_i)$	0.447631	0.461416	0.469388	0.470838	0.476415
$G_t = \sum_i (G_i x_i)(KJ/m^3)$	28	32.54	37.08	41.62	46.16
$E_{M-M} = 2V_t G_t (GPa)$	25.06	30.02	34.80	39.19	43.93
$K_{M-M} = 1.2V_t E_{M-M}(GPa)$	13.46	16.62	19.60	22.14	25.14
$S_{M-M} = (3E_{M-M}K_{M-M})/(9K_{M-M} - E_{M-M})$ (Gpa)	10.53	12.52	14.45	16.26	18.19
$\sigma_{M-M} = \left(\frac{E_{M-M}}{2G_{M-M}}\right) - 1$ (GPa)	0.189	0.198	0.204	0.205	0.208

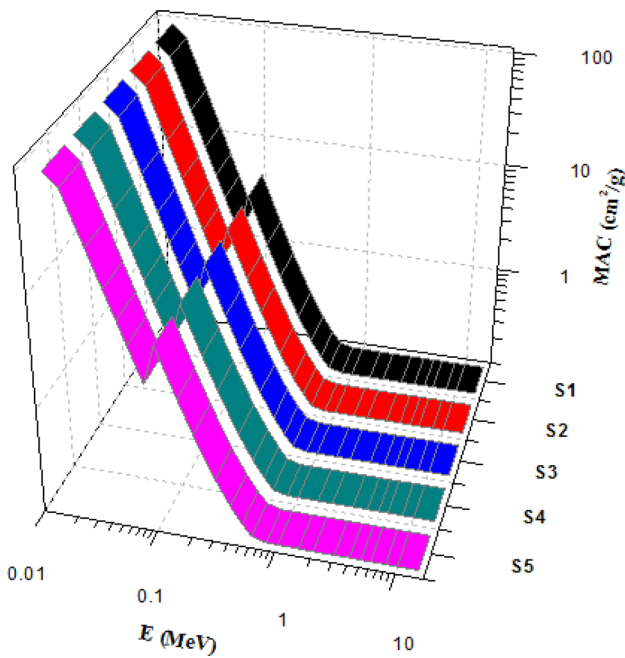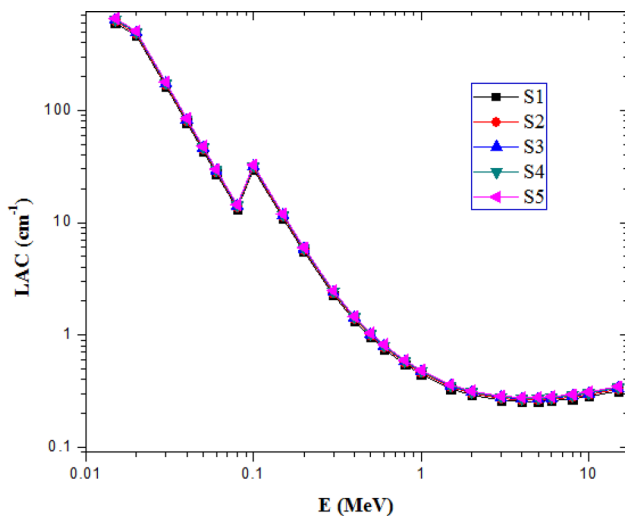**Fig. 3** MAC of S1–S5 glasses as function of photon energy

Fig. 4 Changes in LAC values of S1–S5 glasses as function of photon energy

order of MAC is consistent with that of the mass density. This suggests that MAC values of S1–S5 are linked to their composition. The slight increase in the denser Bi content of the glasses from S1–5 could be the major factor since Bi has a superior MAC compared to the other components in the glass matrix [9, 35, 39].

The values of LAC of the present S-glasses and their variation with photon energy is shown in Fig. 4. This shows that LAC varies with energy in a similar fashion as MAC. Consequently, the highest value of LAC for each of the S-glasses

was obtained at photon energy of 15 keV with values of 601, 624, 640, 648, and 661 cm^{-1} for S1–S5. On the other hand, the smallest values obtained at 4 MeV were 0.255, 0.264, 0.027, 0.0272, and 0.278 cm^{-1} for S1–S5, respectively.

The mean free path (MFP) of photon beam in a medium is the average distance moved by a photon between two successive interactions in the medium [28, 46]. It is a parameter that may be used to compare the photon shielding ability of the medium. Changes in the values of the MFP of photons as a function of photon energy (E) for the glasses is depicted in Fig. 5. The figure shows that MFP rise in value with photon energy up to 4 MeV after which it dropped slightly with increase in E for all the glass samples. As the photon energy rises the probability of interaction reduces consequently, the photon can travel longer distance before interaction. However, as E increased beyond 4 MeV, the dominance of the pair production process sets in. Thus, photons are converted to electron positron pairs which increase their interaction and hence, lowering MFP. The increasing trend of the MFP is opposite to that of MAC and LAC with the order: $(S1)_{MFP}$ > $(S2)_{MFP}$ > $(S3)_{MFP}$ > $(S4)_{MFP}$ > $(S5)_{MFP}$.

Figure 6 shows the variation in the values of TVT with photon energy for all the glasses as calculated from Eq. (5). The TVT is the thickness of the glass needed to reduce photon flux of specified energy to 10%. Like MFP, Fig. 6 shows that TVT increases with E and decreases beyond 4 MeV. This is a sign that more thickness of the glasses is needed to absorb photons of greater energy. The drop in TVT at energies beyond 4 MeV emphasizes the pair production effect at higher energies. Also, TVT of the glasses follow the order $(S1)_{TVT}$ > $(S2)_{TVT}$ > $(S3)_{TVT}$ > $(S4)_{TVT}$ > $(S5)_{TVT}$. The maximum TVT of the glasses was recorded at 4 MeV with values of 3.93, 3.79, 3.70, 3.67, and 3.60 cm for S1, S2, S3, S4, and

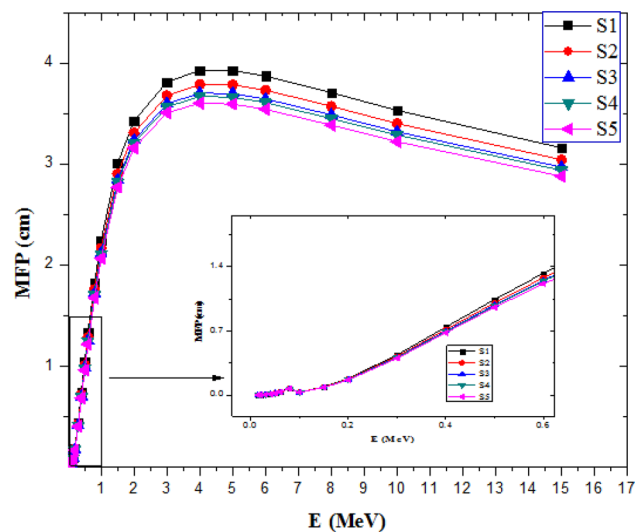**Fig. 5** Variation of MFP with photon energy for S1–S5 glasses
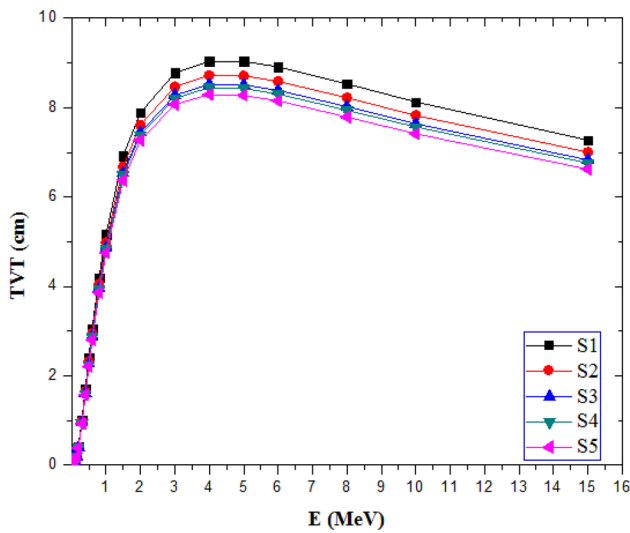
Fig. 6 Variation of TVT values of S1–S5 glasses with photon energy

S5, respectively. Obviously, the slight increase in the relative weight/mole fraction of Bi in the glass from S1 to S5 handles the observed reduction of TVT of the glasses.

To confirm and ascertain the relative photon shielding effectiveness of the $60Bi_2O_3$-$(40-x)$ B_2O_3-$xSiO_2$ glasses in contrast to commercially available glass shields (RS360 and RS520) [59] and a recently investigated glass matrix (TVM60) [28], their HVT were compared at photon energies of 200 and 662 keV as shown in Fig. 7. The HVT is the thickness of the glass needed to reduce photon flux by 50% after interaction. Figure 7 shows that the HVT of S1– S5 were lower than those of the compared material. This is a sign that S1– S5 glasses are better photon absorber and
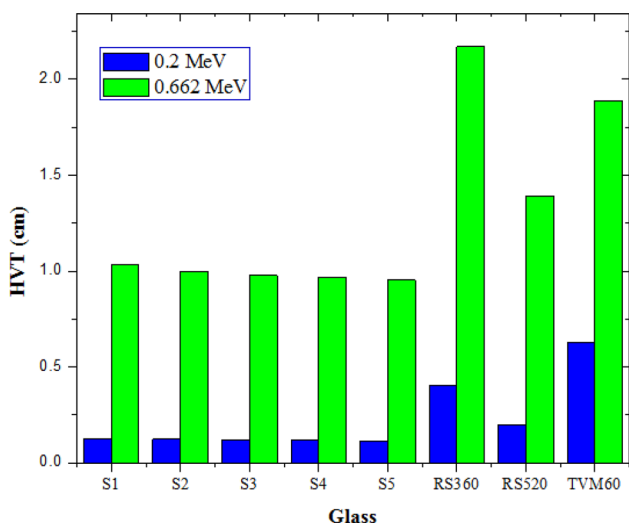
will perform better in gamma radiation shielding in nuclear facilities.

Effective atomic number (Z_{eff}) is a dimensionless quantity that may be used to understand and analyze the interaction of photons of different energies with a medium. Unlike the atomic number (Z) of an element, Z_{eff} varies with photon energy [46]. It also describes the chemical nature of composite material the way Z does and may be used to compare photon interaction in different media. The relationship between values of Z_{eff} of S-glasses and E is presented in Fig. 8. Throughout the energy spectrum, Z_{eff} between 30.64 to 58.42, 31.64 to 59.02, 33.01 to 59.64, 34.32 to 60.31, and 35.75 to 61.02 for S1–S5, respectively. Maximum and minimum value of Z_{eff} was obtained at 0.04 and 1.5 MeV, respectively. for all the glasses, Z_{eff} initially increased with E up to 40 keV; dropped and rose sharply at the K-absorption edge of Bi before gradually dropping as energy increased further. This behavior is a strong sign of the dependence of photon interaction on chemical composition of absorbing material. Figure 8 also showed that at each energy, the trend of the effective atomic number directly follows the MAC. Furthermore, an increase in Bi concentration by mole or weight fraction increased Z_{eff} of the glasses.

Figures 9, 10, 11, 12, 13 show variation of EBUF and EABUF as functions of photon energy for selected penetration depths up to 40 MFP in S1 –S5 glasses. The variations in the values of the buildup factors with respect to energy is similar for all the glasses. The buildup factors sharply increased with energy at Bi atom absorption edges. Generally, both EBUF and EABUF increased with photon energy and depth of penetration except at Bi absorption edges where spikes were seen. Low EBUF and EABUF at the lower energy region is due to the contribution of the
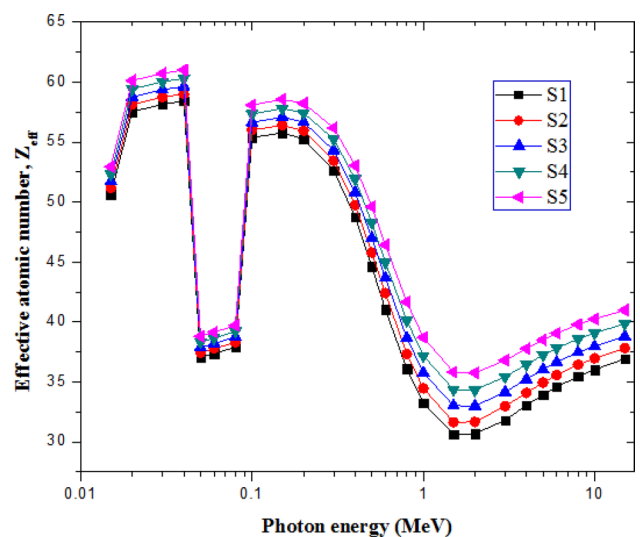

Fig. 7 HVT of S1–S5 glasses compared to other glasses at 0.2 and 0.662 MeV

Fig. 8 Relationship between values of Z_{eff} of S1–S5 glasses and photon energy

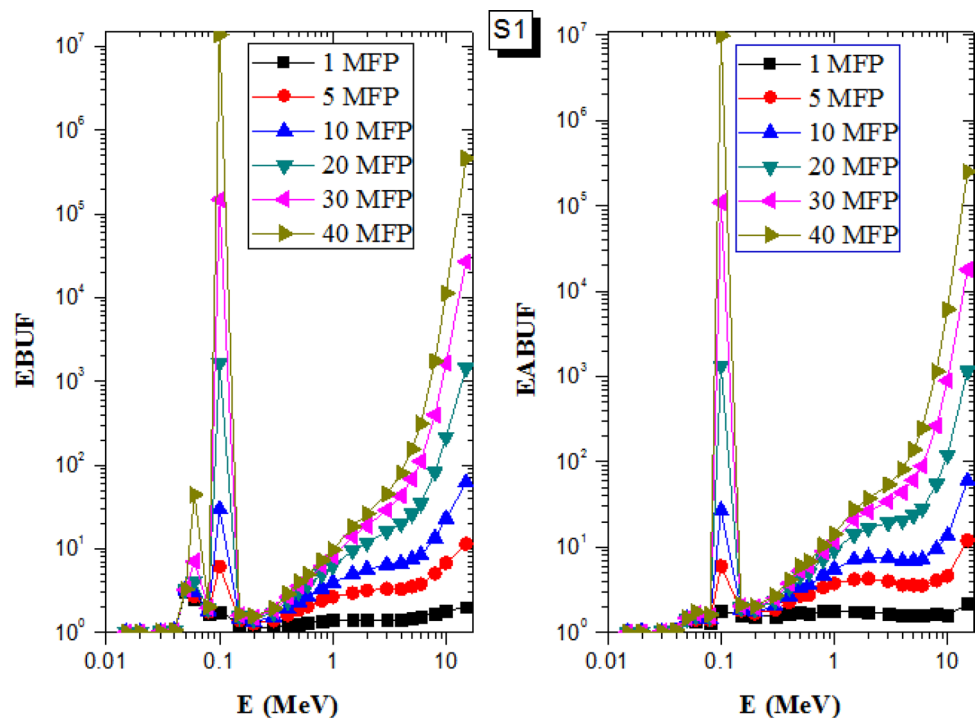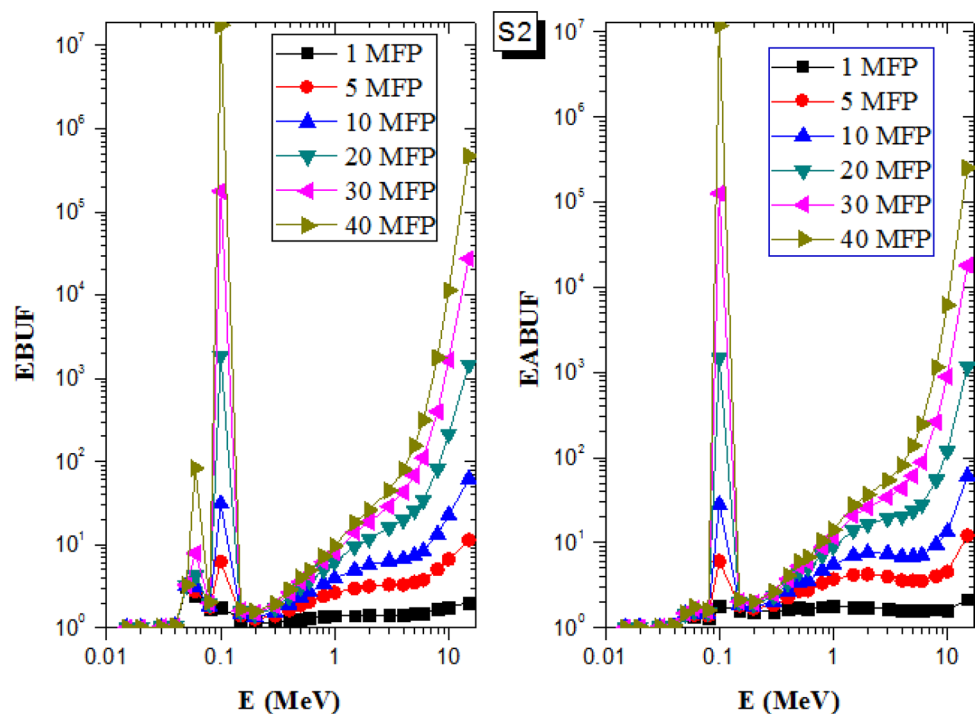**Fig. 9** Variation of EBUF and EABUF of S1 with photon energy

Fig. 10 Variation of EBUF and EABUF of S2 with photon energy

photoelectric absorption process which removes photons and hence prevents buildup. Compton scattering process handles high buildup of photons at energies beyond the photoelectric interaction dominated range. The buildup factors continue to grow to the end of the energy spectrum. Such continuous increase in buildup factors have been seen in materials containing high atomic number composite such as Mo, Pb,

Bi etc. [28, 40, 42, 43]. Figures 14, 15, 16, and 17 show the comparison of EBUF and EABUF S1–S5 glasses at energies of 0.15, 1.5, and 15 MeV as functions of depth. There was a general increase in BUF as the penetration depth increased. Figures also showed that at 0.15 and 15 MeV, there were noticeable differences between the buildup factors of the glasses. However, the differences were more noticeable at

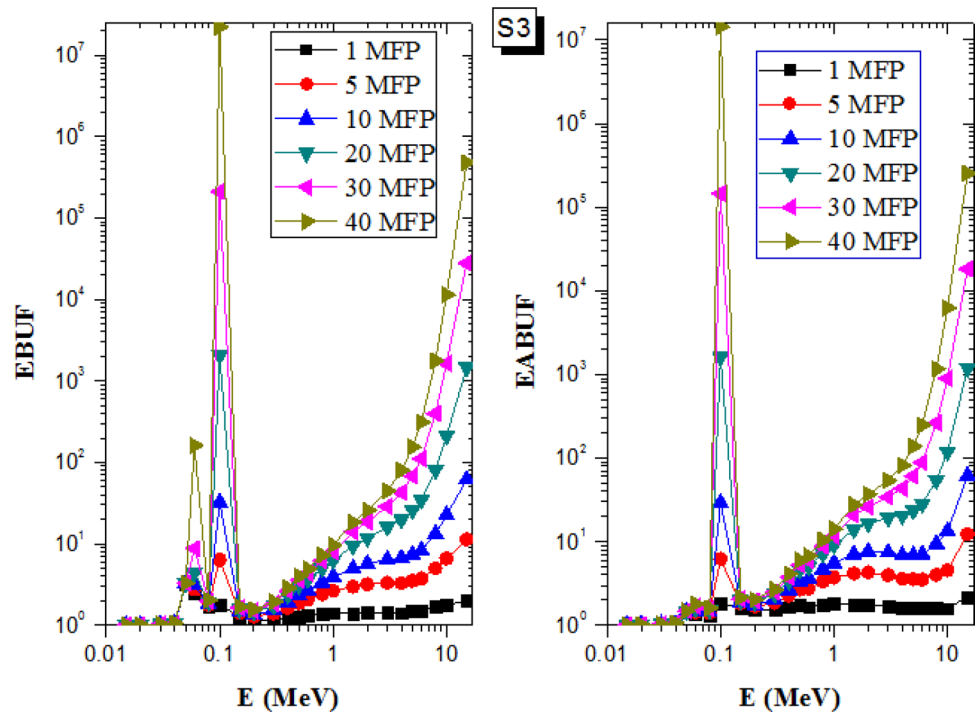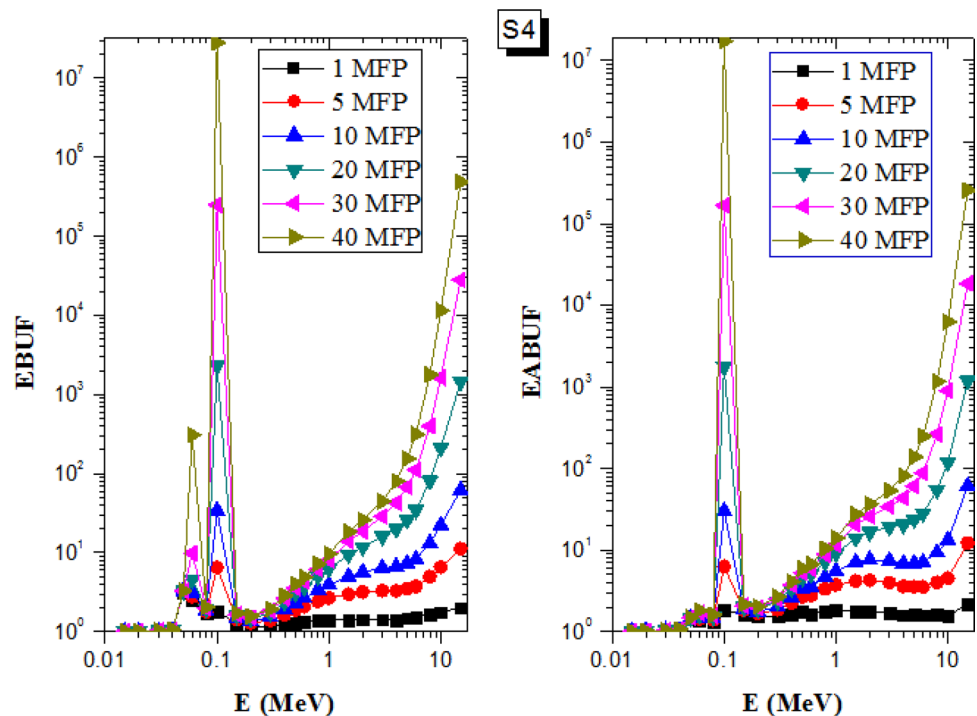**Fig. 11** Variation of EBUF and EABUF of S3 with photon energy

Fig. 12 Variation of EBUF and EABUF of S4 with photon energy

0.15 MeV. This is due to the dominance of photoelectric effect and pair production effect at the energies of 0.15 and 15 MeV, respectively, and their dependence on atomic number. At 1.5 MeV, the buildup factors of the glasses strongly overlapped, a sign that the number of free electrons per mass in the glasses are nearly equal.

Figure 17 presents the effective LAC (ELAC) estimated from Eq. (8) as a function of depth and for 4 selected energies (0.015, 0.15, 1.5 and 15 MeV). The result showed that at 0.015 MeV, ELAC has no noticeable change with respect to depth unlike LAC. Beyond this energy, as the depth increased, ELAC also rose as expected. It therefore means that with a thicker absorber, absorption is higher.

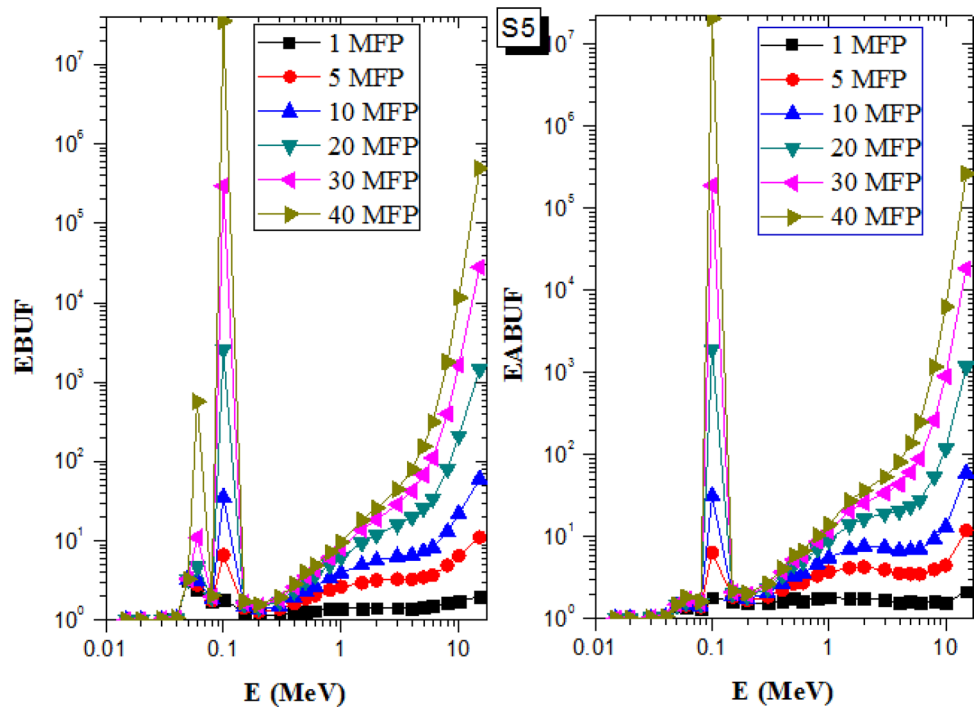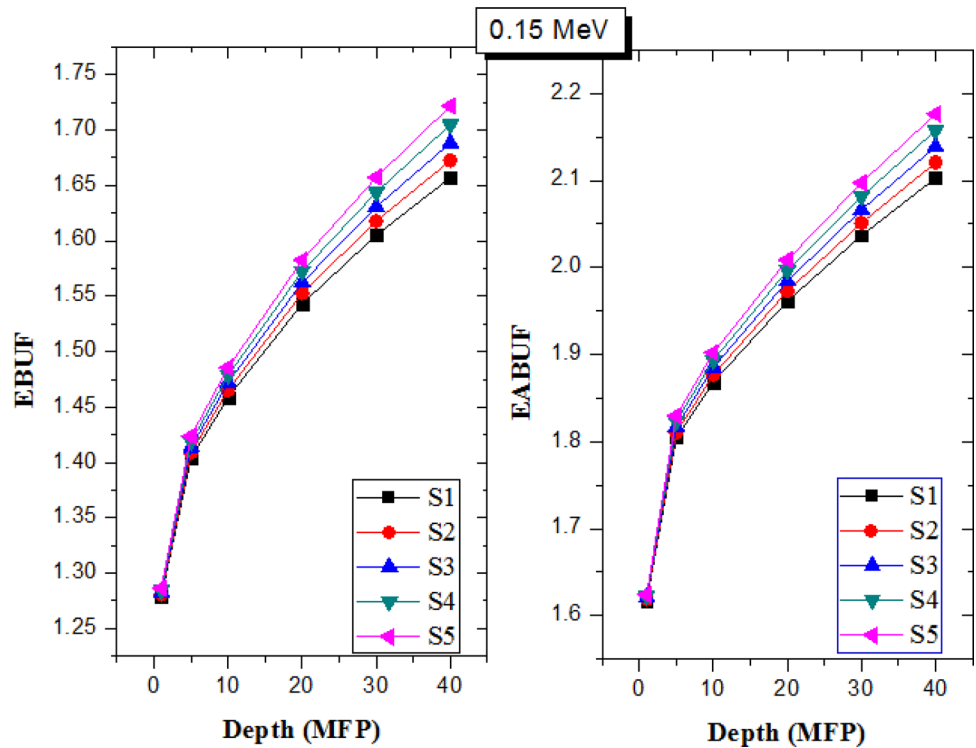**Fig. 13** Variation of EBUF and EABUF of S5 with photon energy

Fig. 14 Variation of EBUF and EABUF of S1–S5 at 0.15 MeV with depth

Comparing the ELAC of the glasses, it is affirmed that S5 has the greatest photon absorption coefficient for all the considered energy and depth. The presence increases in SiO_2 led to a corresponding increase in Bi content in $60Bi_2O_3$-$(40\text{-}x)$ B_2O_3-$xSiO_2$ glasses. This led the observed improved photon absorption ability of the glasses. The consideration of

the BUF in ELAC showed that photon absorption capacity is overestimated when LAC rather than ELAC is used as depicted in Fig. 18. The figure showed the % difference in LAC and ELAC (i.e., $1 - \frac{ELAC}{LAC}$) for all the S-glasses. It can be deduced from the figure that both attenuation coefficients are almost equal at low energies. However, at higher energies

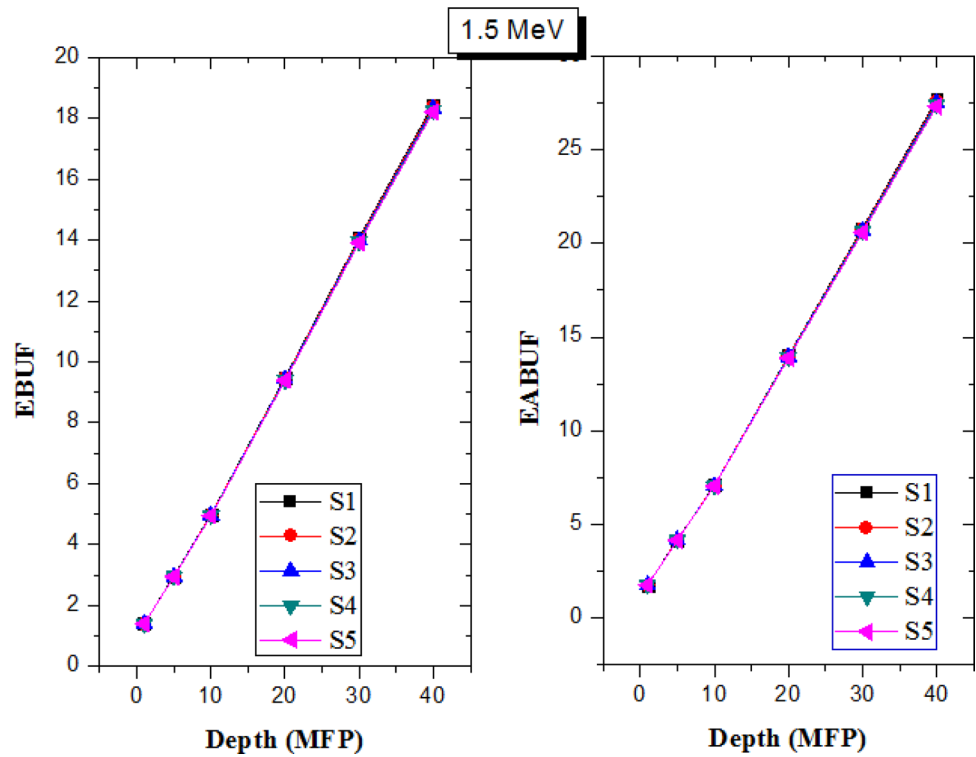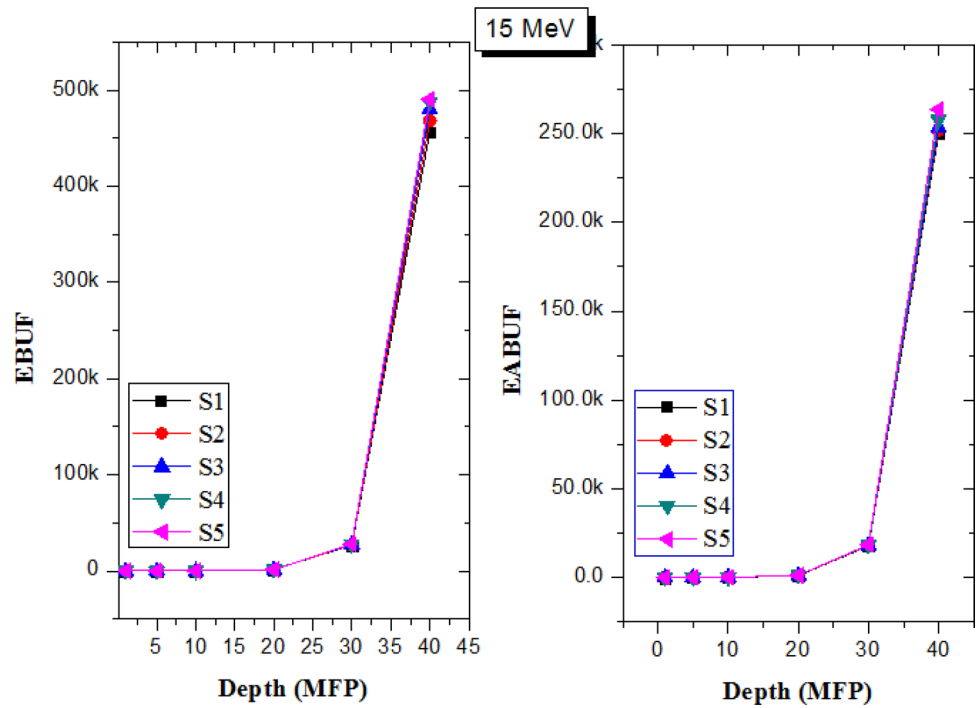**Fig. 15** Variation of EBUF and EABUF of S1–S5 at 1.5 MeV with depth

Fig. 16 Variation of EBUF and EABUF of S1–S5 at 1.5 MeV with depth

and at absorption edges the difference is rather high. The maximum energy of 15 meV, ELAC was less than 30% of LAC.

4.1.1 Neutrons

The macroscopic fast neutron removal cross section (Σ_R) of the S-glasses is presented in Table 4 together with the partial densities of composite elements in the glass system. The
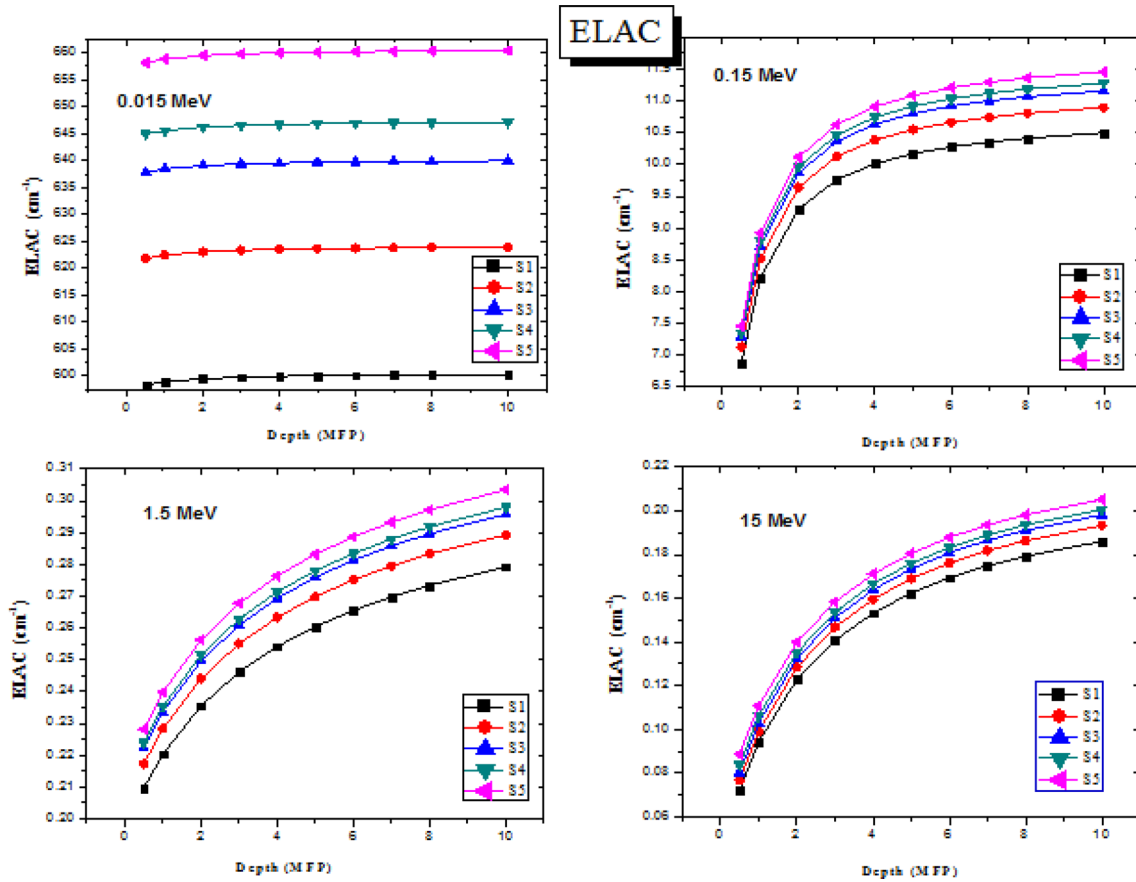
Fig. 17 Comparison of ELAC of S1–S5 at 0.015, 0.15, 1.5, and 15 MeV at different depths
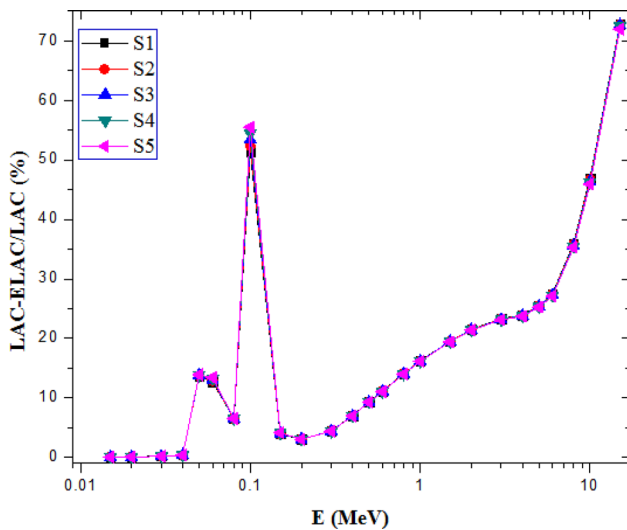

Fig. 18 Relative difference between LAC and ELAC for S1–S5

result showed that Σ_R increased from 0.1033 to 0.105 cm^{-1} for S1–S3 and further reduced S4 and S5 with values of 0.1038 and 0.1034 cm^{-1}, respectively. The increase in Bi atom initially compensated for the reduction in B atom as seen in the increase of the fast neutron removal cross section. However, as the B mass fraction drops beyond that of S3, Σ_R began to reduce. Among the glasses S3 has the optimum Σ_R value among the S-glasses. The value of Σ_R for the S-glasses were better when compared to those of water (0.1024 cm^{-1}), ordinary concrete (OC) (0.094 cm^{-1}) but less than that of TVM60 (0.1055 cm^{-1}) [28], it is obvious that $60Bi_2O_3$-(40-x) B_2O_3-xSiO_2 glasses are poor fast neutron absorber compared TVM60 but better than ordinary concrete and water. The glass system can thus be used for fast neutron absorber rather than ordinary concrete or water.

The presence of B in the $60Bi_2O_3$-(40-x) B_2O_3-xSiO_2 glass system writes down a potential for thermal neutron absorption. This is due to the high thermal neutron absorption ability of B atom. Calculated total thermal neutron cross sections-Σ_T of the glasses are given in Table 5. The table wrote down that Σ_T reduced from 7.95 to 0.31 cm^{-1} as the molar fraction of B_2O_3 reduced from 40 to 0% in the glasses.

Table 5 Partial density, (Σ_R), and total (Σ_R) of S1–S5 glasses

Glass code	Density (g/cm³)	Partial density (g/cm³)				Σ_R(cm⁻¹)				Total Σ_R(cm⁻¹)
		B	O	Si	Bi	B	O	Si	Bi	
S1	6.3298	0.1778	0.988	–	5.1632	0.0102	0.04	–	0.0531	0.1033
S2	6.5527	0.1389	0.992	0.0596	5.362	0.0079	0.0401	0.0016	0.0552	0.1048
S3	6.6948	0.095	0.9814	0.1231	5.495	0.0054	0.0397	0.0034	0.0565	0.105
S4	6.7449	0.0478	0.9564	0.1868	5.5537	0.0027	0.0387	0.0052	0.0572	0.1038
S5	6.855	–	0.9391	0.2536	5.6622	–	0.038	0.0071	0.0583	0.1034

Fig. 19 Total stopping power and CSDA range of electron in S1–S5 as function of energy
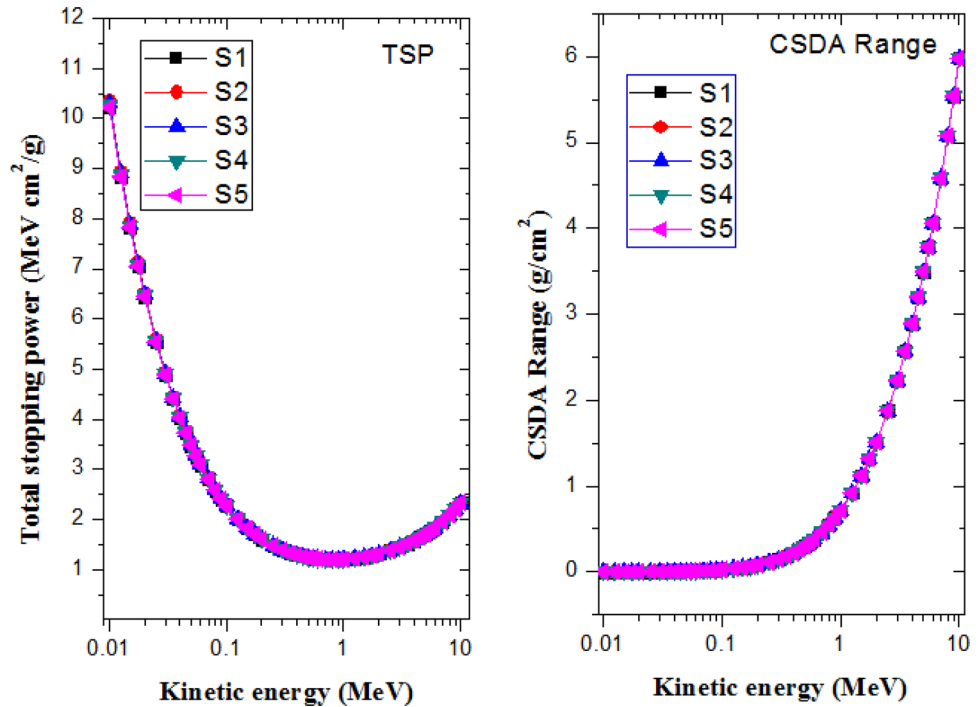
4.1.2 Total stopping powers and range of electron and proton

Figure 19 depicts the total stopping power (TSP) and CSDA range of electrons in the S1–S5 glasses. TSP is an important parameter that may be used for the characterization of charged particle interaction within a medium. TSP is a measure of energy losses by a charged particle per unit thickness of the material due to collision or radiation loses as it travels in the medium. The TSP of electrons in the glasses in variance with kinetic energy is depicted in Fig. 19. From the figure, the TSP decreases smoothly with energy up to kinetic energy of 0.8 MeV. Outside this energy, TSP increased gradually up to the maximum kinetic energy of 10 MeV. The values of TSP at all energy were remarkably close with no significant differences. Also, in the continuous slowing down approximation (CSDA) the electron ranges in

the glasses as functions of energy are also shown in Fig. 19. The range rose with particle kinetic energy all the glasses; showing that higher energy electrons would penetrate deeper in the glasses. The CSDA range of electrons in the glasses at electron energy of 10 MeV was about 5.98 cm²/g in all the glasses. Obviously, there is not much difference between the electron's absorption abilities of S1–S5 glasses.

Figure 20 shows the total mass stopping powers (TMSP) and projected ranges of proton in S1–S5 glasses. TMSP initially increased up to proton energy of 0.09 MeV before decreasing with increase in energy although the TMSP of the glasses were very. Also, the values of projected range (R) of proton generally show an increase with proton energy. This writes down that higher energy protons are more penetrating. Like what obtained of the electrons, the projected range of protons in the glasses is nearly the same (Table 6).

Fig. 20 Total mass stopping power and range of proton in S1–S5 as function of energy
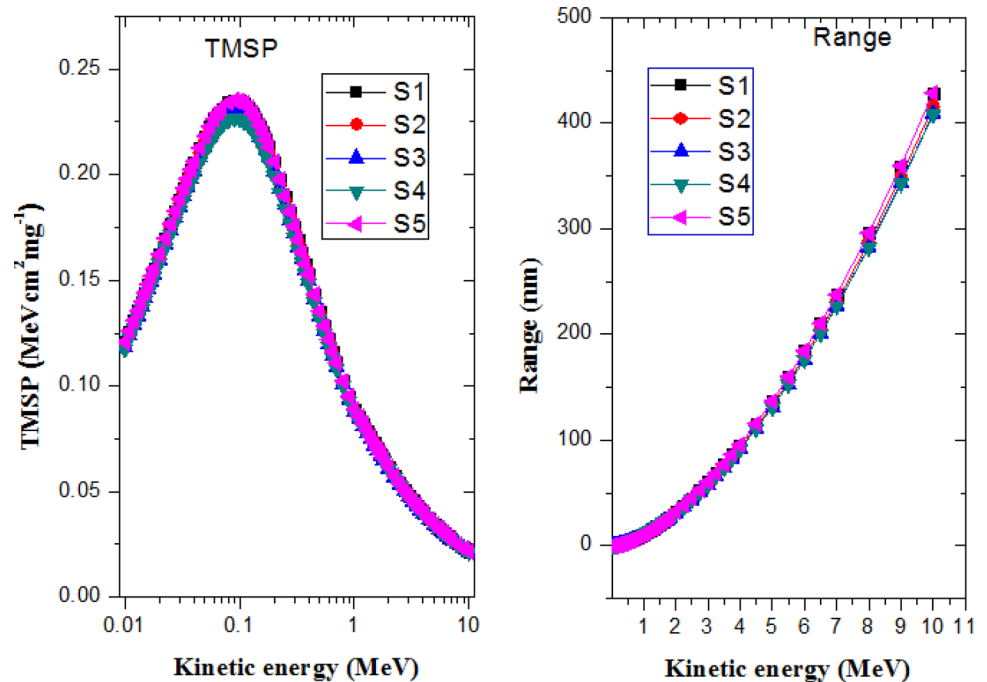

Table 6 Total thermal neutron cross sections (Σ_T) of S1–S5 glasses

Glass code	Density (g/cm³)	Σ_i (cm⁻¹)				Total Σ_T (cm⁻¹)
		B	O	Si	Bi	
S1	6.3298	7.6530	0.1574	0.0000	0.1367	7.9471
S2	6.5527	5.9771	0.1580	0.0029	0.1420	6.2800
S3	6.6948	4.0903	0.1563	0.0061	0.1455	4.3982
S4	6.7449	2.0605	0.1523	0.0093	0.1471	2.3692
S5	6.855	0.0000	0.1496	0.0127	0.1499	0.3122

5 Conclusion

In the present study, the mechanical properties, electron, proton, photon, alpha particle, fast, and thermal neutron shielding capacity of $60Bi_2O_3$-(40-x) B_2O_3-$xSiO_2$ glasses, namely as S1–S5 glasses were investigated and compared with existing shielding glasses. Young's, shear, and longitudinal elastic moduli, and Poisson's ratio have been calculated via bond compression and Makishima–Mackenzie models. Photon shielding parameters of the glasses were mostly influenced by the chemical composition. Higher molar fraction of Bi in the glasses produced better photon shielding coefficients. The increase in the molar fraction of Bi also increased mass density in the glasses. All the S-glasses showed almost similar charged particle shielding ability. On the other hand, the thermal neutron absorption ability of the glasses was dictated by their B content, hence, S1 and S3 was the best thermal and fast neutron absorbing glass. There was no significant difference in the proton and electron shielding abilities of the investigated glasses. The investigated glasses showed superior shielding efficacy when compared with some traditional materials consequently, the S1–S5 glasses are recommended for use as ionizing radiation shields.

References

1. K.A. Matori, M.H.M. Zaid, S.H.A. Aziz, H.M. Kamari, Z.A. Wahab, Study of the elastic properties of (PbO)x(P₂O₅)₁₋ₓ lead phosphate glass using an ultrasonic technique. J. Non-Cryst. Solids **361**, 78–81 (2013)
2. R. Laopaiboon, C. Bootjomchai, Glass structure responses to gamma irradiation using infrared absorption spectroscopy and ultrasonic techniques: a comparative study between Co₂O₃ and Fe₂O₃. Appl. Radiat. Isot. **89**, 42–46 (2014)

3. M.H.M. Zaid, K.A. Matori, H.J. Quah, W.F. Lim, H.A.A. Sidek, M.K. Halimah, W.M.M. Yunus, Z.A. Wahab, Investigation on structural and optical properties of SLS–ZnO glasses prepared using a conventional melt quenching technique. J. Mater. Sci. Mater. Electron. **26**(6), 3722–3729 (2015)

4. T. Yanagida, J. Ueda, H. Masai, Y. Fujimoto, S. Tanabe, Optical and scintillation properties of Ce-doped $34Li_2O$-$5MgO$-$10Al_2O_3$-$51SiO_2$ glass. J. Non-Cryst. Solids **431**, 140–144 (2016)

5. R. Laopaiboon, J. Laopaiboon, S. Pencharee, S. Nontachat, C. Bootjomchai, The effects of gamma irradiation on the elastic properties of soda lime glass doped with cerium oxide. J. Alloys Compd. **666**, 292–300 (2016)

6. K. Kaur, K.J. Singh, V. Anand, Correlation of gamma ray shielding and structural properties of PbO-BaO-P_2O_5 glass system. Nucl. Eng. Des. **285**, 31–38 (2015). https://doi.org/10.1016/j.nucengdes.2014.12.033

7. O. Olarinoye, C. Oche, Gamma-rays and fast neutrons shielding parameters of two new Ti-based bulk metallic glasses, Iranian Journal of. Medical Physics (2020). https://doi.org/10.22038/ijmp.2020.42684.1635

8. M.I. Sayyed, I.A. El-Mesady, A.S. Abouhaswa, A. Askin, Y.S. Rammah, Comprehensive study on the structural, optical, physical and gamma photon shielding features of B_2O_3-Bi_2O_3-PbO-TiO_2 glasses using WinXCOM and Geant4 code. J. Mol. Struct. **1197**, 656–665 (2019)

9. M.S. Al-Buriahi, F.I. El-Agawany, C. Sriwunkum, H. Akyıldırım, H. Arslan, B.T. Tonguc, Y.S. Rammah, Influence of Bi_2O_3/PbO on nuclear shielding characteristics of lead-zinc-tellurite glasses. Physica B **581**, 411946 (2020)

10. M.S. Al-Buriahi, Y.S. Rammah, Investigation of the physical properties and gamma-ray shielding capability of borate glasses containing PbO, Al_2O_3 and Na_2O. Appl. Phys. A **125**, 717 (2019)

11. Y.S. Rammah, M.S. Al-Buriahi, A.S. Abouhaswa, B_2O_3–$BaCO_3$–Li_2O_3 glass system doped with Co_3O_4: structure, optical, and radiation shielding properties. Physica B **576**, 411717 (2020)

12. D.K. Gaikwad, S.S. Obaid, M.I. Sayyed, R.R. Bhosale, V.V. Awasarmol, A. Kumar, M.D. Shirsat, P.P. Pawar, Comparative study of gamma ray shielding competence of WO_3-TeO_2-PbO glass system to different glasses and concretes. Mater Chem. Phys. **213**, 508–517 (2018)

13. C. Bootjomchai, J. Laopaiboon, C. Yenchai, R. Laopaiboon, Gamma-ray shielding and structural properties of barium-bismuth-borosilicate glasses. Radiat. Phys. Chem. **81**, 785–790 (2012). https://doi.org/10.1016/j.radphyschem.2012.01.049

14. A.A.A. Darwish, S.A.M. Issa, M.M. El-Nahass, Effect of gamma irradiation on structural, electrical and optical properties of nano-structure thin films of nickel phthalocyanine. Synth. Methods **215**, 200–206 (2016). https://doi.org/10.1016/j.synthmet.2016.03.002

15. B.O. Elbashir, M.G. Dong, M.I. Sayyed, S.A.M. Issa, K.A. Matori, M.H.M. Zaid, Comparison of Monte Carlo simulation of gamma-ray attenuation coefficients of amino acids with XCOM program and experimental data. Results Phys. **9**, 6–11 (2018). https://doi.org/10.1016/j.rinp.2018.01.075

16. S. Issa, M. Sayyed, M. Kurudirek, Investigation of Gamma Radiation Shielding Properties of Some Zinc Tellurite Glasses. J. Phys. Sci. **27**, 97–119 (2016)

17. S.A.M. Issa, A.A.A. Darwish, M.M. El-Nahass, The evolution of gamma-rays sensing properties of pure and doped phthalocyanine. Prog. Nucl. Energy **100**, 276–282 (2017). https://doi.org/10.1016/j.pnucene.2017.06.016

18. S.A.M. Issa, T.A. Hamdalla, A.A.A. Darwish, Effect of $ErCl_3$ in gamma and neutron parameters for different concentration of $ErCl_3$-SiO_2 (EDFA) for the signal protection from nuclear radiation. J. Alloys Compd. **698**, 234–240 (2017)

19. S.A.M. Issa, Y.B. Saddeek, H.O. Tekin, M.I. Sayyed, K. Saber Shaaban, Investigations of radiation shielding using Monte Carlo method and elastic properties of PbO-SiO_2-B_2O_3-Na_2O glasses. Curr. Appl. Phys. **18**, 717–727 (2018)

20. S.A.M. Issa, M.I. Sayyed, M.H.M. Zaid, K.A. Matori, Photon parameters for gamma-rays sensing properties of some oxide of lanthanides. Results Phys. **9**(2018), 206–210 (2018). https://doi.org/10.1016/j.rinp.2018.02.039

21. S. Kaewjaeng, J. Kaewkhao, P. Limsuwan, U. Maghanemi, Effect of BaO on optical, physical and radiation shielding properties of SiO_2-B_2O_3-Al_2O_3-CaO-Na_2O glasses system. Procedia Eng. **32**, 1080–1086 (2012). https://doi.org/10.1016/j.proeng.2012.02.058

22. R. Mirji, B. Lobo, Computation of the mass attenuation coefficient of polymeric materials at specific gamma photon energies. Phys. Chem. Radiat. **135**, 32–34 (2017). https://doi.org/10.1016/j.radphyschem.2017.03.001

23. K.J. Singh, S. Kaur, R.S. Kaundal, Comparative study of gamma ray shielding and some properties of PbO–SiO_2–Al_2O_3 and Bi_2O_3–SiO_2–Al_2O_3 glass systems. Radiat. Phys. Chem. **96**, 153–157 (2014). https://doi.org/10.1016/j.radphyschem.2013.09.015

24. Y.S. Rammah, F.I. El-Agawany, K.A. Mahmoud, R. El-Mallawany, Erkan Ilik, Gokhan Kilic, FTIR, UV–Vis–NIR spectroscopy, and gamma rays shielding competence of novel ZnO doped vanadium boro phosphate glasses. J. Mater. Sci. Mater. Electron. (2020). https://doi.org/10.1007/s10854-020-03440-5

25. A.A. Ali, Y.S. Rammah, M.H. Shaaban, The influence of TiO_2 on structural, physical and optical properties of B_2O_3 –TeO_2 – Na_2O – CaO glasses. J. Non-Cryst. Solids **514**, 52–59 (2019)

26. Y.S. Rammah, Gökhan Kilic, R. El-Mallawany, U. Gökhan Issever, F.I. El-Agawany, Investigation of optical, physical, and gamma-ray shielding features of novel vanadyl boro-phosphate glasses. J. Non-Cryst. Solids **533**, 119905 (2020)

27. Y.S. Rammah, F.I. El-Agawany, K.A. Mahmoud, A. Novatski, R. El-Mallawany, Role of ZnO on TeO_2. Li_2O ZnO glasses for optical and nuclear radiation shielding applications utilizing MCNP5 simulations and WinXCOM program. J. Non-Cryst. Solids **544**, 120162 (2020)

28. I.O. Olarinoye, F.I. El-Agawany, A. El-Adawy, Y.S. El-Sayed Yousef, Rammah, Mechanical features alpha particles photon proton and neutron interaction parameters of TeO2–V2O3–MoO3 semiconductor glasses. Ceram. Int. (2020). https://doi.org/10.1016/j.ceramint.2020.06.093

29. M.I. Sayyed, H.O. Tekin, O. Kılıcoglu, O. Agar, M.H.M. Zaid, Shielding features of concrete types containing sepiolite mineral: comprehensive study on experimental. XCOM and MCNPX results. Results Phys. **11**, 40–45 (2018). https://doi.org/10.1016/j.rinp.2018.08.029

30. S.H. Elazoumi, H.A.A. Sidek, Y.S. Rammah, R. El-Mallawany, M.K. Halimah, K. Matori, M.H.M. Zaid, Effect of PbO on optical properties of tellurite glass. Results Phys. **8**, 16–25 (2018)

31. M.E. Mahmoud, A.M. El-Khatib, A.M. Halbas, R.M. El-Sharkawy, Investigation of physical, mechanical and gamma-ray shielding properties using ceramic tiles incorporated with powdered lead oxide. Ceram. Int. **46**, 15686–15694 (2020). https://doi.org/10.1016/j.ceramint.2020.03.119

32. R.M. El-Sharkawy, Kh.S. Shaaban, R. Elsaman, E.A. Allam, A. El-Taher, M.E. Mahmoud, Investigation of mechanical and radiation shielding characteristics of novel glass systems with the composition xNiO-20ZnO-60B_2O_3-(20–x) CdO based on nanometal oxides. J. Non-Cryst. Solids **528**, 119754 (2020). https://doi.org/10.1016/j.jnoncrysol.2019.119754

33. M.S. Al-Buriahi, Y.S. Rammah, Electronic polarizability, dielectric, and gamma-ray shielding properties of some tellurite-based glasses. Appl. Phys. A **125**(10), 678 (2019)

34. F.I. El-Agawany, E. Kavaz, U. Perişanoğlu, M.S. Al-Buriahi, Y.S. Rammah, Sm_2O_3 effects on mass stopping power/projected range

and nuclear shielding characteristics of TeO_2–ZnO glass systems. Appl. Phys. A **125**, 838 (2019)

35. Y.S. Rammah, M.I. Sayyed, A.A. Ali, H.O. Tekin, R. El-Mallawany, Optical properties and gamma shielding features of bismuth borate glasses. Appl. Phys. A **124**, 824–832 (2018)

36. M.I. Sayyed, Investigations of gamma ray and fast neutron shielding properties of tellurite glasses with different oxide compositions. Can. J. Phys. **94**(11), 1133–1137 (2016)

37. E. Kavaz, N. Ekinci, H.O. Tekin, M.I. Sayyed, B. Aygün, U. Perişanoğlu, Estimation of gamma radiation shielding qualification of newly developed glasses by using WinXCOM and MCNPX code. Prog. Nucl. Energy **115**, 12–20 (2019)

38. Y.S. Rammah, H.O. Tekin, C. Sriwunkum, I. Olarinoye, A. Alalawi, M.S. Al-Buriahi, T. Nutaro, B.T. Tonguc, Investigations on borate glasses within SBC-Bx system for gamma-ray shielding applications. Nucl. Eng. Technol. (2021). https://doi.org/10.1016/j.net.2020.06.034

39. M.I. Sayyed, Bismuth modified shielding properties of zinc borotellurite glasses. J. Alloy. Compd. **688**, 111–117 (2016)

40. B.O. El-Bashir, M.I. Sayyed, M.H.M. Zaid, K.A. Matori, Comprehensive study on physical, elastic and shielding properties of ternary BaO-Bi_2O_3-P_2O_5 glasses as a potent radiation shielding material. J. Non-Cryst. Solids **468**, 92–99 (2017)

41. M.I. Sayyed, K.M. Kaky, D.K. Gaikwad, O. Agar, U.P. Gawai, S.O. Baki, Physical, structural, optical and gamma radiation shielding properties of borate glasses containing heavy metals (Bi_2O_3/MoO_3). J. Non-Cryst. Solids **507**, 30–37 (2019)

42. S.A. Issa, H.O. Tekin, R. Elsaman, O. Kilicoglu, Y.B. Saddeek, M.I. Sayyed, Radiation shielding and mechanical properties of Al_2O_3-Na_2O-B_2O_3-Bi_2O_3 glasses using MCNPX Monte Carlo code. Mater. Chem. Phys. **223**, 209–219 (2019)

43. Y.S. Rammah, I.O. Olarinoye, F.I. El-Agawany, A. El-Adawy, A. Gamal, El Sayed Yousef, Elastic moduli, photon, neutron, and proton shielding parameters of tellurite bismo-vanadate (TeO_2–V_2O_5–Bi_2O_3) semiconductor glasses. Ceram. Int. (2020). https://doi.org/10.1016/j.ceramint.2020.07.014

44. M.M. Gomaa, S. Ibrahim, H. Darwish, Effect of SiO_2/B_2O_3 replacements on the structure, physicochemical and electrical properties of Bi_2O_3-containing glasses. Silicon **7**, 55–63 (2015)

45. N. Elkhoshkhany, E. Syala, E. Yousef, Concentration dependence of the elastic moduli, thermal properties, and non-isothermal kinetic parameters of Yb^{3+} doped multicomponent tellurite glass system. Results Phys. **16**, 102876 (2020)

46. I. Olarinoye, Variation of effective atomic numbers of some thermoluminescence and phantom materials with photon energies. Res J Chem Sci. **1**(2), 64–69 (2011)

47. L. Gerward, N. Guilbert, K.B. Jensen, H. Levring, X-ray absorption in matter. Reengineering XCOM. Radiat Phys. Chem. **60**, 23–24 (2001)

48. I.O. Olarinoye, Photon buildup factors for some tissues and phantom materials for penetration depths up to 100 MFP. J. Nucl. Res. Dev. **13**, 57–67 (2017)

49. I.O. Olarinoye, R.I. Odiaga, S. Paul, EXABCal: A program for calculating photon exposure and energy absorption buildup factors. Heliyon **5**(7), e02017 (2019)

50. E. Şakar, Ö.F. Özpolat, B. Alım, M.I. Sayyed, M. Kurudirek, Phy-X/PSD: development of a user friendly online software for calculation of parameters relevant to radiation shielding and dosimetry. Radiat. Phys. Chem. **166**, 108496 (2020)

51. F.H. Attix, *Introduction to Radiological Physics and Radiation Dosimetry* (Wiley, New Jersey, 2008).

52. A. El-Khayatt, Calculation of fast neutron removal cross-sections for some compounds and materials. Ann. Nucl. Energy **37**(2), 218–222 (2010)

53. F.A. Schmidt, *Attenuation Properties of Concrete for Shielding of Neutrons of Energy Less than 15 MeV (No ORNL-RSIC-26)* (Oak Ridge National Lab, Tenn, 1970).

54. V.F. Sears, Neutron scattering lengths and cross sections. Neutron News **3**, 29–37 (1992)

55. T. Korkut, V.V. Çay, M. Sütçü, O. Gencel, Neutron radiation tests about Fe-Cr slag and natural zeolite loaded brick samples. Sci. Technol. Nucl. Ins. **2014**, 190–193 (2014)

56. G. Lakshminarayana, I. Kebaili, M.G. Dong, M.S. Al-Buriahi, A. Dahshan, I.V. Kityk, T. Park, Estimation of gamma-rays, and fast and the thermal neutrons attenuation characteristics for bismuth tellurite and bismuth boro-tellurite glass systems. J. Mat. Sci. **55**(14), 5750–5771 (2020)

57. J.F. Ziegler, M.D. Ziegler, J.P. Biersack, SRIM - the stopping and range of ions in matter. Nucl. Instrum. Methods B **268**, 1818–1823 (2010)

58. M.J. Berger, J.S. Coursey, M.A. Zucker, J. Chang. Stopping-power and range tables for electrons, protons, and helium ions, Gaithersburg, MD: NIST Physics Laboratory (2017). http://physics.nist.gov/Star

59. ⟨http://www.schott.com/advanced_optics/english/products/optical-materials/special-materials/radiation-shielding-glasses/index.html⟩